Structural Transition of Gold Nanoclusters: From the Golden Cage to the Golden Pyramid

Wei Huang,[†] Satya Bulusu,[‡] Rhitankar Pal,[‡] Xiao Cheng Zeng,[‡,*] and Lai-Sheng Wang[†,*]

[†]Department of Physics, Washington State University, 2710 University Drive, Richland, Washington 99354, Chemical & Materials Sciences Division, Pacific Northwest National Laboratory, MS K8-88, P.O. Box 999, Richland, Washington 99352, and [‡]Department of Chemistry and Center for Materials and Nanoscience, University of Nebraska—Lincoln, Lincoln, Nebraska 68588

ABSTRACT How nanoclusters transform from one structural type to another as a function of size is a critical issue in cluster science. Here we report a study of the structural transition from the golden cage Au_{16}^- to the pyramidal Au_{20}^-. We obtained distinct experimental evidence that the cage-to-pyramid crossover occurs at Au_{18}^-, for which the cage and pyramidal isomers are nearly degenerate and coexist experimentally. The two isomers are observed and identified by their different interactions with O_2 and Ar. The cage isomer is observed to be more reactive with O_2 and can be preferentially "titrated" from the cluster beam, whereas the pyramidal isomer has slightly stronger interactions with Ar and is favored in the $Au_{18}Ar_x^-$ van der Waals complexes. The current study allows the detailed structural evolution and growth routes from the hollow cage to the compact pyramid to be understood and provides information about the structure—function relationship of the Au_{18}^- cluster.

KEYWORDS: gold clusters · photoelectron spectroscopy · structural isomers · van der Waals complexes · structure—function relationship

Gold is the most inert metal in the periodic table. However, at nanometer scale, supported gold particles have been shown to display a remarkable repertoire of catalytic activities.[1] This discovery has stimulated a renaissance of investigations on the structures and properties of gaseous gold clusters, which provide atomically defined models for understanding the mechanisms of the catalytic effects of gold nanoparticles. A diverse set of structures has been observed experimentally and proposed theoretically for a variety of gold clusters. In particular, the structures of gold cluster anions Au_n^- in the size range from $n = 3$ to 20 have been well-established using a combination of experimental techniques and density functional theory (DFT) calculations, ranging from the planar (2D) clusters for $n < 13$,[2] the tetrahedral Au_{20}^-,[3] and the cage clusters for $n = 16-18$.[4] The 2D Au_n^- clusters were first discovered in an ion mobility experiment[2] and have been confirmed by both photoelectron spectroscopy (PES)[5] and trapped ion electron diffraction (TIED) experiment.[6] However, the 2D-to-3D transition has been controversial[7] and is only resolved recently in a combined TIED and DFT study.[8] Both the Au_{16}^- cage and the Au_{20}^- pyramid have been confirmed in a series of experimental and theoretical studies,[6,9−15] but how the clusters evolve from the cage to the pyramidal structure has not been understood. In the initial PES/DFT study,[4] Au_{16}^- and Au_{17}^- were shown definitively to be cages, whereas Au_{19}^- was shown to be pyramidal, similar to Au_{20}^-. The global minimum of Au_{18}^- was concluded to be a cage, but the PES spectrum of Au_{18}^- suggested the presence of another minor isomer, which could be interpreted by either cage-like structures or a pyramidal structure. Thus, no definitive assignment was possible. A subsequent PES/DFT study confirmed the presence of isomers in Au_{18}^- and suggested that the PES data contain a mixture of cage and pyramidal structures.[9] However, using the same theoretical data, a simultaneous TIED/DFT study assigned Au_{18}^- to the pyramidal structure.[6] Recent catalytic studies suggest that supported gold nanoparticles in the size range of 10−20 atoms may be the active species.[16] Hence, understanding the structures and structural transitions of gold clusters in this size range is of critical importance.

Because of the theoretical challenges presented by gold clusters as a result of the strong relativistic and spin−orbit effects,[8,17] definitive experimental data are essential in helping elucidate their structures and chemical reactivity. In particular, in cases of multiple isomers, it is critical to be able to identify contributions from different isomers and to obtain isomer-specific chemical and spectroscopic information. This is especially true when there is a

*Address correspondence to xczeng@phase2.unl.edu, ls.wang@pnl.gov.

Received for review March 7, 2009 and accepted April 09, 2009.

Published online April 16, 2009. 10.1021/nn900232d CCC: $40.75

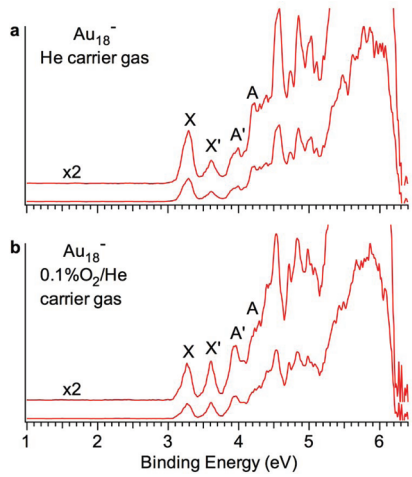

Figure 1. Photoelectron spectra of Au_{18}^- at 193 nm (6.424 eV), (a) with a pure helium carrier gas, (b) with a helium carrier gas seeded with 0.1% O_2.

structural transition, where isomers from different structure types may become degenerate and coexist experimentally, such as the 2D-to-3D crossover at Au_{12}^-.[2] On the other hand, different structures may exhibit different chemical and physical properties, which can be used to provide isomer-specific information. Recently, we have shown that the main isomer of Au_{10}^-, which is a D_{3h} triangle, is not reactive with O_2, whereas minor isomers of Au_{10}^- are reactive with O_2 and can be titrated out to produce a clean D_{3h} Au_{10}^- beam.[18] We have also observed that planar Au_n^- clusters (including the pyramidal Au_{20}^-) have stronger van der Waals interactions with Ar and used this property to obtain isomer-specific PES spectra for Au_{12}^-.[19] We found that Ar can titrate out the 2D Au_{12}^- isomer from the beam, whereas the $Au_{12}Ar_x^-$ complexes contain a larger proportion of the 2D isomer.

In the current article, we use the O_2 titration and Ar tagging to probe the structural transition from the golden cages starting at Au_{16}^- to the pyramidal structure in Au_{20}^-. We found that the crossover size is Au_{18}^-, for which both the cage and pyramidal isomers coexist experimentally. The cage isomer is observed to be slightly more reactive with O_2, while the pyramidal isomer has slightly stronger interactions with Ar, similar to Au_{20}^-.[19] These different chemical and physical properties are used to provide definitive isomer information. The confirmation of the two coexisting isomers at Au_{18}^- in conjunction with a detailed structural analysis provides an atom-by-atom view about the growth routes and structural transitions from the golden cage to the golden pyramid.

O_2 Titration. Figure 1a shows the 193 nm photoelectron spectrum of Au_{18}^- produced using a laser vaporization cluster source with a pure helium carrier gas and taken using a magnetic bottle PES apparatus (see Methods).[20] This spectrum is the same as that reported before.[4] The threshold peak X at a vertical detachment energy (VDE) of 3.32 eV was assigned to the cage structure, whereas the weaker features X′ (VDE = 3.63 eV) and A′ (VDE = 3.97 eV) were suggested to originate from another minor isomer. Previous chemical studies[21−23] showed that for small Au_n^- clusters ($n < 24$) only even-sized clusters are reactive with O_2 (except Au_{16}^-) because the even-sized Au_n neutral clusters are closed shell and the corresponding anions possess relatively low electron binding energies[24] so that the extra electron can be transferred to O_2 to form chemisorbed $Au_nO_2^-$ complexes. Using a helium carrier gas seeded with a 0.1% O_2, we found that indeed, in the size range from Au_{16}^- to Au_{19}^-, only Au_{18}^- reacts with O_2 to form a $Au_{18}O_2^-$ complex, in agreement with the previous works.[21−23] However, the photoelectron spectrum of the unreacted portion of the Au_{18}^- beam with the 0.1% O_2/He carrier gas was very different from that taken with a pure helium carrier gas, as shown in Figure 1b: the X′ and A′ peaks were greatly enhanced and became even stronger than the X band. This observation indicates that the X′ and A′ features indeed come from a Au_{18}^- isomer, which is less reactive with O_2 than the global minimum cage isomer. This is understandable because the electron binding energy (VDE = 3.32 eV) of the cage isomer is lower than the X′ isomer (VDE = 3.63 eV), and thus it is expected to be easier for it to transfer an electron to O_2. At a higher O_2 concentration (0.5%), we found that the majority of the Au_{18}^- beam is converted to $Au_{18}O_2^-$, suggesting that the X′ isomer of Au_{18}^- is also reactive with O_2, preventing us from obtaining an isomer-clean spectrum for the low-lying isomer. The Au_{18}^- case is different from Au_{10}^-, for which we were able to use a 0.5% O_2/He carrier gas to completely titrate out reactive isomers to yield an isomer-clean D_{3h} Au_{10}^- spectrum because the D_{3h} Au_{10}^- isomer is inert toward O_2.[18]

Ar Tagging. The question now is what is the minor isomer observed for Au_{18}^-? In our original PES/DFT study,[4] this was not definitively answered because several low-lying isomers, including the pyramidal isomer, seemed to give PES bands consistent with the X′ and A′ features. A subsequent PES/DFT study yielded similar structures for Au_{18}^- and suggested similarly that the spectrum of Au_{18}^- consists most likely of a combination of low-lying isomers, including the ground state cage isomer, the pyramidal isomer, and another higher-lying cage structure.[9] However, a simultaneous TIED study using the same DFT result concluded that the pyramidal Au_{18}^- fits best the TIED data.[6] Because of the pairwise additive nature of the van der Waals interactions between a rare gas atom and a cluster,[25] a 2D structure is expected to have stronger interactions with Ar than a 3D structure of the same cluster size. This was recently observed to be the case for all 2D Au_n^- clusters, which exhibit a strong propensity to form van der Waals complexes with Ar.[19] The pyramidal Au_{20}^- cluster was also shown to readily form $Au_{20}Ar_x^-$ complexes because of

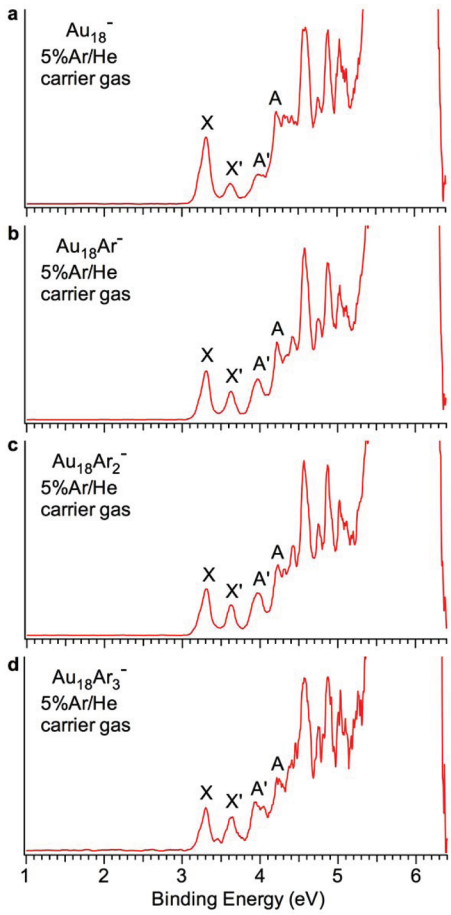

Figure 2. Comparison of the 193 nm photoelectron spectrum of Au_{18}^- with those of Ar-physisorbed clusters $Au_{18}Ar_x^-$ ($x = 1-3$). (a) Spectrum of Au_{18}^- with a helium carrier gas seeded with 5% Ar. (b) Spectrum of $Au_{18}Ar^-$. (c) Spectrum of $Au_{18}Ar_2^-$. (d) Spectrum of $Au_{18}Ar_3^-$. Note the reduction of the relative intensities of the weak features (X′ and A′) in (a) and their increases in the spectra of the Ar-tagged species from $x = 1-3$.

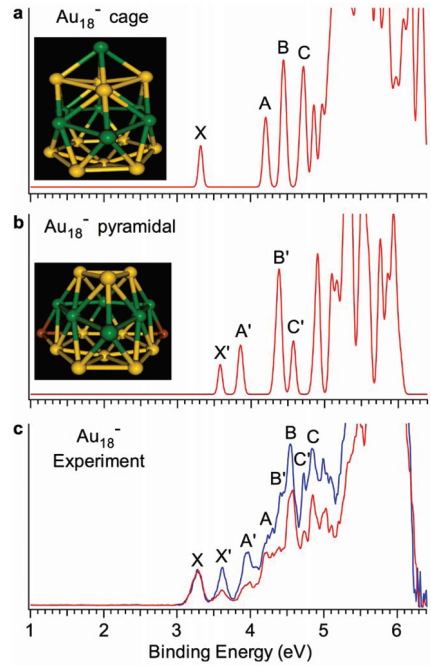

Figure 3. Comparison of simulated spectra with the experimental photoelectron spectra of Au_{18}^-. (a) Simulated spectrum for the cage isomer.[4] (b) Simulated spectrum for the pyramidal isomer from.[4] (c) Photoelectron spectra of Au_{18}^- from Figure 1 plotted together by normalizing to the first band X. Note the increase of the relative intensities of the X′, A′, B′, and C′ bands under the O_2 titration condition (blue), which correspond to the pyramidal isomer.

its four Au(111) faces.[3] Similar effects were observed previously in $Xe-Au_n^-$ complexes.[26] If the minor isomer of Au_{18}^- is pyramidal, we may be able to use Ar tagging to distinguish it because it should have a stronger interaction with Ar than the cage structure. This has indeed been observed, as shown in Figure 2.

Figure 2a shows a Au_{18}^- spectrum taken with a 5% Ar/He carrier gas, under which $Au_{18}Ar_x^-$ van der Waals complexes are readily formed in our cluster source. The relative intensities of the X′ and A′ bands are clearly reduced (also see Figure S1 in the Supporting Information). The ratio of the X′ to X peak intensities decreased to ~0.30 in the spectrum using the 5% Ar/He carrier gas compared to ~0.44 under a pure He carrier gas (Figure 1a). This decrease was due to a titration effect by Ar, which preferentially forms van der Waals complexes with the pyramidal isomer, as observed very prominently for Au_{20}^-.[19] This was borne out more evidently in the spectra of the $Au_{18}Ar_x^-$ van der Waals complexes (Figure 2b–d). The spectra of the $Au_{18}Ar_x^-$ van der Waals complexes are nearly identical to the pure Au_{18}^- spectrum without any spectral shifts within our experimental accuracy, due to the weak interactions between Ar and Au_{18}^-, which does not change the electronic or geometric structures of the Au_{18}^- parent. However, the relative intensities of X′ and A′ increase with the number of Ar atoms attached. The intensity ratio of the X′ to X peaks increases to ~0.58 in $Au_{18}Ar^-$, ~0.65 in $Au_{18}Ar_2^-$, and ~0.78 in $Au_{18}Ar_3^-$ (Figure S1 in Supporting Information). These observations provide definitive evidence for the coexistence of the pyramidal isomer. Its planar surfaces induce slightly stronger interactions with Ar than the cage structure and are thus preferentially formed in the $Au_{18}Ar_x^-$ van der Waals complexes.

The relative intensities of the X′ and A′ peaks remain constant under different conditions, indicating that they both come from the pyramidal isomer. The X′ and A′ separation yields an energy gap of 0.34 eV for the pyramidal isomer. Similarly, the ratio of the X and A bands remains constant under different conditions, suggesting that the A band represents the second PES transition for the cage isomer and yielding an energy gap of 0.90 eV. The lower electron binding energy and larger energy gap of the Au_{18}^- cage isomer are the origins of its relatively higher reactivity with O_2.

Comparison with Simulated Spectra for the Cage and Pyramidal Structures of Au_{18}^-. To further confirm the assignment of the pyramidal isomer, we compare the simulated spectra for the cage and pyramidal structures with the new isomer-dependent PES data in Figure 3. As dis-

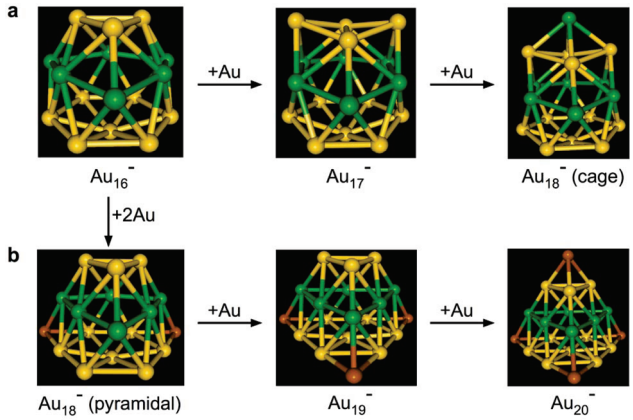

Figure 4. Growth pathways from the hollow Au_{16}^- cage to the close-packed Au_{20}^- pyramid: (a) cage route; (b) pyramidal route.

cussed previously,[4] the ground state cage structure is in excellent agreement with the observed main isomer (Figure 3a), in particular, the X and A bands. Similarly, the current data show that the simulated spectra for the pyramidal isomer (Figure 3b), in particular, the X′ and A′ bands, are in quantitative agreement with the corresponding experimental features. The observed spectra between 4 and 5 eV are quite congested due to the overlap of PES features from the two isomers (Figure 3c). Nevertheless, comparison of the isomer-dependent data in Figure 3c allows us to assign several higher binding energy peaks (*i.e.*, B and C for the cage isomer and B′ and C′ for the pyramidal isomer). We should point out that none of the other isomers reported from the previous DFT study[4] are in such good agreement with the observed spectra.

The experimental evidence from O_2 titration and Ar tagging and the excellent agreement between the simulated and the observed isomer-dependent spectra confirm unequivocally that the cage and pyramidal isomers coexist for Au_{18}^-. Theoretical calculations[4,9] predict that the pyramidal isomer is slightly higher in energy by ~0.02−0.05 eV than the global minimum cage isomer. This also agrees with the fact that under normal conditions the intensity of the X band from the cage isomer is higher than the X′ band from the pyramidal isomer, meaning the cage isomer should be slightly more stable than the pyramidal isomer. Our previous work shows that the global minimum of Au_{17}^- is the cage structure without any close-lying isomers, whereas the pyramidal structure is overwhelmingly the global minimum for Au_{19}^-.[4] Thus, Au_{18}^- is unquestionably the crossover size between the cage and pyramidal structures, which are nearly degenerate and coexist experimentally at $n = 18$ even under relatively cold experimental conditions. This behavior is similar to the 2D-to-3D transition at Au_{12}^-, for which both isomers are nearly degenerate and coexist at $n = 12$, with the 3D isomer slightly more stable than the 2D structure.[2,8,19]

Structure Evolution from the Au_{16}^- Cage to the Au_{20}^- Pyramid. The next question is how the cage structures evolve to the pyramidal structures. What is the intrinsic link between Au_{16}^- and Au_{20}^-? Historically, the pyramidal Au_{20}^- was discovered first,[3] and the structure of the Au_{16}^- cage was found later.[4] The golden cage Au_{16}^- has been viewed as removing the four apex atoms from the pyramidal Au_{20}^- while simultaneously popping up the face-center atoms (see Figure 4). The pyramidal Au_{20}^- cluster is close-packed, similar to bulk gold, and possesses four Au(111) faces. While Au_{16}^- maintains the tetrahedral symmetry of the parent Au_{20}^-, the popping up of the four face-center atoms created a central volume and a distinctly hollow cage structure in Au_{16}^-, which has been shown to be able to entrap a variety of external atoms analogous to the fullerenes.[27−31]

Origin of the Hollow Golden Cage Au_{16}^-: Spherical Aromaticity. Recent chemical bonding analyses[32,33] show that the pyramidal Au_{20} can be described by 10 four-center two-electron (4c-2e) bonds localized on 10 intertwining Au_4 tetrahedra. More importantly, the closed-shell Au_{16}^{2-} cage has been shown to contain three globally delocalized 16c-2e bonds derived from its triply degenerate frontier orbital, in addition to six 4c-2e bonds.[33] We note that the three globally delocalized 16c-2e bonds are responsible for the caging in Au_{16}^{2-} because removal of these three electron pairs promptly returns the Au_{16}^{4+} cluster to a compact T_d structure,[33] which is an exact fragment of Au_{20} by removing the four corner atoms. The six globally delocalized electrons in Au_{16}^{2-} give rise to spherical aromaticity, which is also analogous to the fullerenes.[34] The spherical aromaticity provides extra electronic stability and explains the unique hollow cage structure in the Au_{16}^- and Au_{16}^{2-} golden cages. The idea of spherical aromaticity has been proposed for other larger gold cage clusters suggested computationally.[35−43] Apparently, the removal of one electron from Au_{16}^{2-} does not destroy the spherical aromaticity in Au_{16}^-, but the removal of two electrons seems to destroy the spherical aromaticity in the neutral Au_{16} because the global minimum of the neutral Au_{16} is no longer the cage structure.[44]

Cage Growth: From Au_{16}^- to Au_{17}^-. However, in reality, the pyramidal clusters grow from the Au_{16}^- cage by nucleation of additional Au atoms. Figure 4 delineates two growth pathways from Au_{16}^-: the cage growth route (Figure 4a) and the pyramidal path (Figure 4b). To help visualize the structures and understand the growth path, the atoms are color-coded in Figure 4. The Au_{16}^- cage can be viewed as consisting of three layers. The bottom layer contains a six-membered ring with one central atom, which is out of plane, giving rise to the curvature for the cage (note that Au_{16}^- possesses tetrahedral symmetry, and there are three more such atoms in the green-colored middle layer). This layer is related to the Au_{20}^- base plane. The middle layer (green color) contains six atoms to form a six-membered ring,

which is related to the second layer of Au_{20}^- (similarly colored, Figure 4b). The top layer of Au_{16}^- is a triangle, which can be viewed as due to the truncation of an apex atom from Au_{20}^-. The ground state structure of Au_{17}^- is formed by adding a Au atom into the top layer of Au_{16}^- with a slight rearrangement to give a butterfly four-atom top layer (Figure 4a), whereas the bottom and middle layers are essentially unaffected relative to Au_{16}^-. Our previous work showed that the structure along the pyramidal growth route by adding a Au atom to the top triangular site of Au_{16}^- is much less stable.[4]

From Au_{17}^- to Au_{18}^-: Cage or Pyramid? Addition of a capping atom to the top layer of Au_{17}^- leads to the ground state Au_{18}^- cage (Figure 4a). The butterfly top layer of Au_{17}^- is slightly distorted, but the bottom and second layers are again essentially unaffected in the Au_{18}^- cage relative to those in Au_{16}^- and Au_{17}^-. However, in Au_{18}^-, the pyramidal structure becomes competitive and nearly degenerate with the cage. The pyramidal structure of Au_{18}^- is formed by adding two atoms to the bottom layer of the Au_{16}^- cage (Figure 4). Note that the addition of these apex atoms induces a significant "de-caging" effect, considerably flattening the four atoms that give rise to the curvature in the Au_{16}^- cage. These four atoms transform naturally to the face centers of the pyramidal Au_{20}^-. The flattening effect in the Au_{18}^- pyramidal structure is directly responsible for the enhanced van der Waals interactions with Ar, relative to the cage isomer.

Addition of one more apex atom to the pyramidal Au_{18}^- structure further flattens the structure and leads to a very stable pyramidal Au_{19}^- (Figure 4b), for which the cage isomer derived from the Au_{18}^- cage becomes much less stable according to our previous DFT calculations.[4] Addition of one more apex atom to Au_{19}^- produces a perfect tetrahedral Au_{20}^- with four Au(111) faces and completes the cage-to-pyramid evolution from Au_{16}^- to Au_{20}^-.

CONCLUSIONS

The current study shows that chemical titration and van der Waals complex formation are effective techniques to deconvolute complex photoelectron spectra of size-selected clusters due to coexisting isomers at major structural transitions, thereby providing critical structural and isomeric information. Such information is crucial in comparing with computational results in order to elucidate the size-dependent structures and structural evolution of clusters. Both electronic and atomic structures are important in determining the novel chemical and physical properties of nanoclusters. The present results reveal that the higher O_2 reactivity of the Au_{18}^- cage isomer is distinctly an electronic effect. Detailed structures of supported gold catalysts are still elusive. Thus, continued progress in understanding the structures of size-selected gold nanoclusters and the structure−function relationships will be important in the understanding of the catalytic effects of gold and may suggest new strategies to design more efficient catalysts.

METHODS

The experiment was carried out with a magnetic bottle photoelectron spectroscopy apparatus equipped with a laser vaporization cluster source, details of which has been reported elsewhere.[20] A gold disk target was vaporized by a pulsed laser to generate a plasma inside a cluster nozzle with a large waiting room. A high-pressure helium carrier gas pulse was delivered to the nozzle simultaneously, cooling the plasma and initiating nucleation. Clusters formed inside the nozzle were entrained in the helium carrier gas and underwent a supersonic expansion for further cooling. After a skimmer, anions from the collimated cluster beam were extracted perpendicularly into a time-of-flight mass spectrometer. Clusters of interest were selected by a mass-gate and decelerated before being photodetached by a 193 nm laser beam from an ArF excimer laser. Photoelectrons were collected by a magnetic bottle at nearly 100% efficiency into a 3.5 m long electron flight tube for kinetic energy analyses. The photoelectron kinetic energies were calibrated by the known spectra of Au^- and subtracted from the photon energies to obtain the reported electron binding energy spectra. The electron kinetic energy (E_k) resolution of our apparatus is $\Delta E_k/E_k \sim 2.5\%$ (*i.e.*, ~25 meV for 1 eV electrons).

As shown previously,[45,46] by carefully controlling the resident time of the clusters in the nozzle, relatively cold clusters can be produced from our laser vaporization supersonic cluster source. The cooling effects have been confirmed recently by the observation of van der Waals clusters of gold cluster anions with Ar.[18,19] In the present study, the $Au_{18}Ar_x^-$ clusters were produced using a helium carrier gas seeded with 5% Ar. For the O_2 titration experiment, a 0.1% O_2/He carrier gas was used.

Acknowledgment. The experimental work done at Washington was supported by the National Science Foundation (CHE-0749496) and was performed at the EMSL, a national scientific user facility sponsored by the DOE's Office of Biological and Environmental Research and located at the Pacific Northwest National Laboratory, operated for DOE by Battelle. The theoretical work done at Nebraska was supported by grants from the National Science Foundation (CHE-0427746, DMR/MRSEC-0820521), the Nebraska Research Initiative, and the UNL Research Computing Facility and Holland Supercomputing Center at University of Nebraska—Omaha.

Supporting Information Available: Intensity ratios of the X′ to the X band in the Au_{18}^- spectra under different experimental conditions and that in the Ar−Au_{18}^- van der Waals complexes. This material is available free of charge *via* the Internet at http://pubs.acs.org.

REFERENCES AND NOTES

1. Haruta, M. Size- and Support-Dependency in the Catalysis of Gold. *Catal. Today* **1997**, *36*, 153–166.
2. Furche, F.; Ahlrichs, R.; Weis, P.; Jacob, C.; Gilb, S.; Bierweiler, T.; Kappes, M. M. The Structures of Small Gold Cluster Anions as Determined by a Combination of Ion Mobility Measurements and Density Functional Calculations. *J. Chem. Phys.* **2002**, *117*, 6982–6990.
3. Li, J.; Li, X.; Zhai, H. J.; Wang, L. S. Au_{20}^-: A Tetrahedral Cluster. *Science* **2003**, *299*, 864–867.
4. Bulusu, S.; Li, X.; Wang, L. S.; Zeng, X. C. Evidence of Hollow Golden Cages. *Proc. Natl. Acad. Sci. U.S.A.* **2006**, *103*, 8326–8330.

5. Hakkinen, H.; Yoon, B.; Landman, U.; Li, X.; Zhai, H. J.; Wang, L. S. On the Electronic and Atomic Structures of Small Au_N^- ($N = 4-14$) Clusters: A Photoelectron Spectroscopy and Density-Functional Study. *J. Phys. Chem. A* **2003**, *107*, 6168–6175.
6. Xing, X.; Yoon, B.; Landman, U.; Parks, J. H. Structural Evolution of Au Nanoclusters: From Planar to Cage to Tubular Motifs. *Phys. Rev. B* **2006**, *74*, 165423.
7. Koskinen, P.; Hakkinen, H.; Huber, B.; von Issendorff, B.; Moseler, M. Liquid−Liquid Phase Coexistence in Gold Clusters: 2D or Not 2D? *Phys. Rev. Lett.* **2007**, *98*, 015701.
8. Johansson, M. P.; Lechtken, A.; Schooss, D.; Kappes, M. M.; Furche, F. 2D−3D Transition of Gold Cluster Anions Resolved. *Phys. Rev. A* **2008**, *77*, 053202.
9. Yoon, B.; Koskinen, P.; Huber, B.; Kostko, O.; von Issendorff, B.; Hakkinen, H.; Moseler, M.; Landman, U. Size-Dependent Structural Evolution and Chemical Reactivity of Gold Clusters. *ChemPhysChem* **2007**, *8*, 157–161.
10. Lechtken, A.; Neiss, C.; Stairs, J.; Schooss, D. Comparative Study of the Structures of Copper, Silver, and Gold Isomers: Influence of Metal Type and Charge State. *J. Chem. Phys.* **2008**, *129*, 154304.
11. Gruene, P.; Rayner, D. M.; Redlich, B.; van der Meer, A. F. G.; Lyon, J. T.; Meijer, G.; Fielicke, A. Structures of Neutral Au_7, Au_{19}, and Au_{20} Clusters in the Gas Phase. *Science* **2008**, *321*, 674–676.
12. Fernández, E. M.; Soler, J. M.; Garzón, I. L.; Balbás, L. C. Trends in the Structure and Bonding of Noble Metal Clusters. *Phys. Rev. B* **2004**, *70*, 165403.
13. Apra, E.; Ferrando, R.; Fortunelli, A. Density-Functional Global Optimization of Gold Nanoclusters. *Phys. Rev. B* **2006**, *73*, 205414.
14. Kryachko, E. S.; Remacle, F. The Magic Gold Cluster Au_{20}. *Int. J. Quantum Chem.* **2007**, *107*, 2922–2934.
15. Krishnamurty, S.; Shafai, G. S.; Kanhere, D. G.; Soule de Bas, B.; Ford, M. J. *Ab Initio* Molecular Dynamical Investigation of the Finite Temperature Behavior of the Tetrahedral Au_{19} and Au_{20} Clusters. *J. Phys. Chem. A* **2007**, *111*, 10769–10775.
16. Herzing, A. A.; Kiely, C. J.; Carley, A. F.; Landon, P.; Hutchings, G. J. Identification of Active Gold Nanoclusters on Iron Oxide Supports for CO Oxidation. *Science* **2008**, *321*, 1331–1335.
17. Pyykko, P. Relativistic Effects in Structural Chemistry. *Chem. Rev.* **1988**, *88*, 563–594.
18. Huang, W.; Wang, L. S. Au_{10}^-: Isomerism and Structure-Dependent O_2 Reactivity. *Phys. Chem. Chem. Phys.* **2009**, *11*, 2663–2667.
19. Huang, W.; Wang, L. S. Probing the 2D to 3D Structural Transition in Gold Cluster Anions Using Argon Tagging. *Phys. Rev. Lett.* **2009**, 102.
20. Wang, L. S.; Cheng, H. S.; Fan, J. W. Photoelectron Spectroscopy of Size-Selected Transition-Metal Clusters: Fe_n^-, $n = 3-24$. *J. Chem. Phys.* **1995**, *102*, 9480–9493.
21. Cox, D. M.; Brickman, R.; Creegan, K.; Kaldor, A. Gold Clusters: Reactions and Deuterium Uptake. *Z. Phys. D: At. Mol. Clusters* **1991**, *19*, 353–355.
22. Salisbury, B. E.; Wallace, W. T.; Whetten, R. L. Low-Temperature Activation of Molecular Oxygen by Gold Clusters: A Stoichiometric Process Correlated to Electron Affinity. *Chem. Phys.* **2000**, *262*, 131–141.
23. Stolcic, D.; Fischer, M.; Gantefor, G.; Kim, Y. D.; Sun, Q.; Jena, P. Direct Observation of Key Reaction Intermediates on Gold Clusters. *J. Am. Chem. Soc.* **2003**, *125*, 2848–2849.
24. Taylor, K. J.; Pettiettehall, C. L.; Cheshnovsky, O.; Smalley, R. E. Ultraviolet Photoelectron Spectra of Coinage Metal Clusters. *J. Chem. Phys.* **1992**, *96*, 3319–3329.
25. Bruch, L. W.; Cole, M. W.; Zaremba, E. *Physical Adsorption: Forces and Phenomena*; Oxford University Press: Oxford, 1997.
26. Gilb, S.; Jacobsen, K.; Schooss, D.; Furche, F.; Ahlrichs, R.; Kappes, M. M. Electronic Photodissociation Spectroscopy of Au_n^-Xe ($n = 7-11$) *versus* Time-Dependent Density Functional Theory Prediction. *J. Chem. Phys.* **2004**, *121*, 4619–4627.
27. Walter, M.; Hakkinen, H. A Hollow Tetrahedral Cage of Hexadecagold Dianion Provides a Robust Backbone for a Tuneable Sub-Nanometer Oxidation and Reduction Agent *via* Endohedral Doping. *Phys. Chem. Chem. Phys.* **2006**, *8*, 5407–5411.
28. Gao, Y.; Bulusu, S.; Zeng, X. C. A Global Search of Highly Stable Gold-Covered Bimetallic Clusters $M@Au_n$ ($n = 8-17$): Endohedral Gold Clusters. *ChemPhysChem* **2006**, *7*, 2275–2278.
29. Wang, L. M.; Bulusu, S.; Huang, W.; Pal, R.; Wang, L. S.; Zeng, X. C. Doping the Golden Cage Au_{16}^- with Si, Ge, and Sn. *J. Am. Chem. Soc.* **2007**, *129*, 15136–15137.
30. Wang, L. M.; Bai, J.; Lechtken, A.; Huang, W.; Schooss, D.; Kappes, M. M.; Zeng, X. C.; Wang, L. S. Magnetic Doping of the Golden Cage Cluster $M@Au_{16}^-$ (M = Fe, Co, Ni). *Phys. Rev. B* **2009**, *79*, 033413.
31. Wang, L. M.; Pal, R.; Huang, W.; Zeng, X. C.; Wang, L. S. Tuning the Electronic Properties of the Golden Buckyball by Endohedral Doping: $M@Au_{16}-$(M = Ag, Zn, In). *J. Chem. Phys.* **2009**, *130*, 051101.
32. King, R. B.; Chen, Z.; Schleyer, P. v. R. Structure and Bonding in the Omnicapped Truncated Tetrahedral Au_{20} Cluster: Analogies between Gold and Carbon Cluster Chemistry. *Inorg. Chem.* **2004**, *43*, 4564–4566.
33. Zubarev, D. Y.; Boldyrev, A. I. Deciphering Chemical Bonding in Golden Cages. *J. Phys. Chem. A* **2009**, *113*, 866–868.
34. Buhl, M.; Hirsch, A. Spherical Aromaticity of Fullerenes. *Chem. Rev.* **2001**, *101*, 1153–1184.
35. Johansson, M. P.; Sundholm, D.; Vaara, J. Au_{32}: A 24-Carat Golden Fullerene. *Angew. Chem., Int. Ed.* **2004**, *43*, 2678–2681.
36. Gu, X.; Ji, M.; Wei, S. H.; Gong, X. G. Au_N clusters ($N = 32$, 33, 34, 35): Cagelike Structures of Pure Metal Atoms. *Phys. Rev. B* **2004**, *70*, 205401.
37. Gao, Y.; Zeng, X. C. Au_{42}: An Alternative Icosahedral Golden Fullerene Cage. *J. Am. Chem. Soc.* **2005**, *127*, 3698–3699.
38. Wang, J.; Jellinek, J.; Zhao, J.; Chen, Z.; King, R. B.; Schleyer, P. v. R. Hollow Cages *versus* Space-Filling Structures for Medium-Sized Gold Clusters: The Spherical Aromaticity of the Au_{50} Cage. *J. Phys. Chem. A* **2005**, *109*, 9265–9269.
39. Fa, W.; Luo, C.; Dong, J. Bulk Fragment and Tubelike Structures of Au_N ($N = 2-26$). *Phys. Rev. B* **2005**, *72*, 205428.
40. Tian, D.; Zhao, J.; Wang, B.; King, R. B. Dual Relationship between Large Gold Clusters (Antifullerenes) and Carbon Fullerenes: A New Lowest-Energy Cage Structure for Au_{50}. *J. Phys. Chem. A* **2007**, *111*, 411–414.
41. Sun, Q.; Wang, Q.; Jena, P.; Kawazoe, Y. Design of Janus Nanoparticles with Atomic Precision: Tungsten-Doped Gold Nanostructures. *ACS Nano* **2008**, *2*, 341–347.
42. Karttunen, A. J.; Linnolahti, M.; Pakkanen, T.; Pyykko, P. Icosahedral Au_{72}: A Predicted Chiral and Spherically Aromatic Golden Fullerene. *Chem. Commun.* **2008**, 465–467.
43. Johansson, M. P.; Vaara, J.; Sundholm, D. Exploring the Stability of Golden Fullerenes. *J. Phys. Chem. C* **2008**, *112*, 19311–19315.
44. Bulusu, S.; Zeng, X. C. Structures and Relative Stability of Neutral Gold Clusters: Au_n ($n = 15-19$). *J. Chem. Phys.* **2006**, *125*, 154303.
45. Akola, J.; Manninen, M.; Hakkinen, H.; Landman, U.; Li, X.; Wang, L. S. Photoelectron Spectra of Aluminum Cluster Anions: Temperature Effects and *Ab Initio* Simulations. *Phys. Rev. B* **1999**, *60*, R11297–R11300.
46. Wang, L. S.; Li, X. Temperature Effects in Anion Photoelectron Spectroscopy of Metal Clusters. In *Clusters and Nanostructure Interfaces*; Jena, P., Khanna, S. N., Rao, B. K., Eds; World Scientific: River Edge, NJ, 2000; pp 293−300.